Enhancing Regional Jet Efficiency with Truss-Braced Wings: An Improvement on the Embraer ERJ145

Israel Demandel *
Yale University, New Haven, Connecticut, United States, 06511

The sustainability of aviation is necessary to reduce carbon emissions and the effects of climate change. This study examines the aerodynamic performance of Truss-Braced Wings (TBWs) and their potential applications in improving the L/D of incompressible and transonic aircraft. It is determined that adding a truss increases the pressure coefficient near the leading edge, which is reduced by increasing the aspect ratio. Moreover, optimal performance is achieved with truss location towards the quarter and mid-S_T region at the transonic flight regime. The combination of truss location and aspect ratio optimizes performance in incompressible and transonic regimes. This study highlights the importance of balancing the aspect ratio and truss location to achieve the desired pressure coefficient values. These findings have implications for guiding aircraft design in both regimes, with potential benefits for electric aircraft and transonic regional aircraft performance.

Disclaimer

This study was conducted over a six-week period from July 6 to August 17, 2024. The limitations and outcomes of this research may reflect the constraints inherent to this timeframe. Despite rigorous efforts to ensure accuracy and thoroughness, the conclusions drawn are contingent upon the specific conditions and scope of the research undertaken during this period. Future investigations may yield additional insights or developments beyond those presented in this study.

Nomenclature

α	Angle of Attack
γ	Ratio of Specific Heats
μ	Dynamic Viscosity
ρ	Density of fluid
A	Axial Force
A_W	Wetted Area
AoA	Angle of Attack
c	Chord
Cd	Drag Coefficient
CFD	Computational Fluid Mechanics
Cl	Lift Coefficient
Cp	Pressure Coefficient
FVM	Finite Volume Method
L/D	Lift-to-Drag Ratio
L	Characteristic Length
Ma	Mach Number
N	Normal Force
p	Pressure
p_∞	Pressure of Free Stream
R	Gas Constant
Re	Reynold's Number
S_T	Location in X/Span for Truss
T	Absolute Temperature
TBW	Truss Braced Wing
$TOGW$	Take Off Gross Weight
v	Fluid Velocity
X	X Location of Local Coordinates
x	Cartesian Coordinate in x
X_i	Vertices Location of Local Coordinates in X
Y	Y Location of Local Coordinates
Y_i	Vertices Location of Local Coordinates in Y
Z	Z Location of Local Coordinates
Z_i	Vertices Location of Local Coordinates in Z

*Undergraduate Student, Yale College

I. Introduction

Sustainable aviation is essential for achieving net-zero emissions and mitigating the effects of climate change. It primarily encompasses three areas: propulsion, structures, and airline operations [1]. This paper focuses on the structural aspect of sustainable aircraft technology, particularly in light of recent developments by Boeing and the National Aeronautics and Space Administration (NASA) in the Subsonic Ultra Green Aircraft Research (SUGAR) project [2, 3]. The SUGAR project has demonstrated promising advances in sustainability by improving the lift-to-drag (L/D) ratio and reducing wing weight [2, 3]. These improvements highlight the need for substantial changes to the conventional tube-and-wing design to achieve notable reductions in fuel consumption. Specifically, the L/D coefficient is of great interest since increasing it can lead to reduced fuel consumption.

This paper explores the potential application of TBWs in an existing regional aircraft, the Embraer ERJ145. This aircraft is commonly used for regional flights in the United States, which constitute 41% of total U.S. flights [4]. Focusing on regional jets could lead to significant reductions in carbon emissions. Moreover, the focus on regional aircraft arises from the limited research on TBW technology and its application in these aircraft.

II. Background

A. Truss-Braced Wings

The concept of a TBW dates back to the 1970s and was first proposed by Pfenninger [5]. The basic design is shown in Figure 1, in which the wing features a strut arm with jury supports (i.e., the vertical supports). TBWs allow for an increase in the aspect ratio of the wings (i.e., the wings become slender) through structural support due to greater wing flexibility. TBWs offer various advantages such as having a path for commercial integration and significantly improving the L/D [2, 3]. However, there are potential unknowns regarding the full scope as to how TBWs behave such as the local aerodynamics between the main wing and the supporting structure.

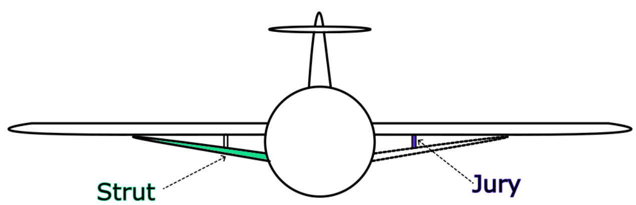

Fig. 1 Truss braced wing aircraft inspired by Pfenninger [5]

The SUGAR project incorporated Pfenninger's early design into the Boeing 737-class airplane structure. In particular, the SUGAR project researched different designs as shown in Figure 2. Additional jury members allow for increased stiffness. However, the increased number of jury members causes increased weight. Seber et al analyzed different configurations of the Boeing 777-200ER and found that the take-off gross weight (TOGW), fuel weight, and wing weight are all less than the conventional cantilever wing [6]. These results show promise in TBW technology; it reduces fuel consumption by having an overall lighter plane which improves the sustainability of airplanes. Moreover, Seber et al show that the TBW design allows for an increased aspect ratio (AR) [6]; therefore, the induced drag can be reduced which increases L/D [7].

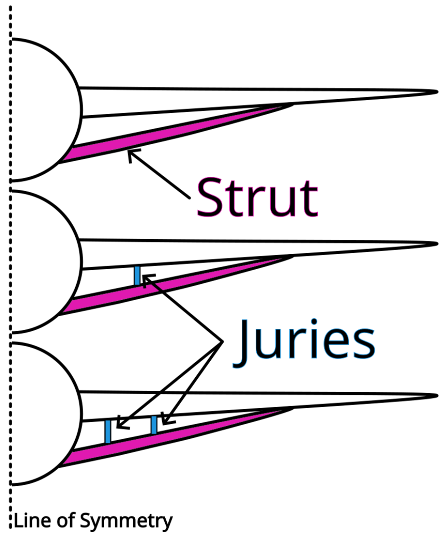

Fig. 2 Various TBW configurations inspired by Chakraborty et al [8]

Nevertheless, there are unknowns regarding the airflow surrounding the jury, particularly near the junction between the wing and the jury. One of the goals of this paper is to understand the aerodynamics surrounding the junction to provide insights for future TBW development. In particular, Ivaldi et al describes the risk of reverse flow near the junction of the wing and strut [9]. Furthermore, there is a lack of definitions for describing spatial relationships between the junction, the strut, and the wing [9]. Therefore, this paper aims to produce definitions for spatial relationships between the strut and wing. In turn, these spatial definitions will promote an understanding of aerodynamic concepts like lift, drag, or coefficient of pressure. Understanding the previously mentioned concepts can be achieved through an analysis of forces acting on an airfoil.

B. Aerodynamics of Wings

The main forces of interest to understand an airfoil are lift and drag. As the names suggest, lift is the force that allows an aircraft to rise and must exceed the aircraft's TOGW. Drag, on the other hand, opposes the horizontal motion of the aircraft, counteracting the engine thrust. These forces are influenced by the angle of attack, which is the angle between the chord line and the direction of the free stream velocity (see Figure 3). The chord line is defined as the straight line between the trailing edge (back) and the leading edge (front) of the airfoil [10]. The free stream refers to the air that is far from the airfoil.

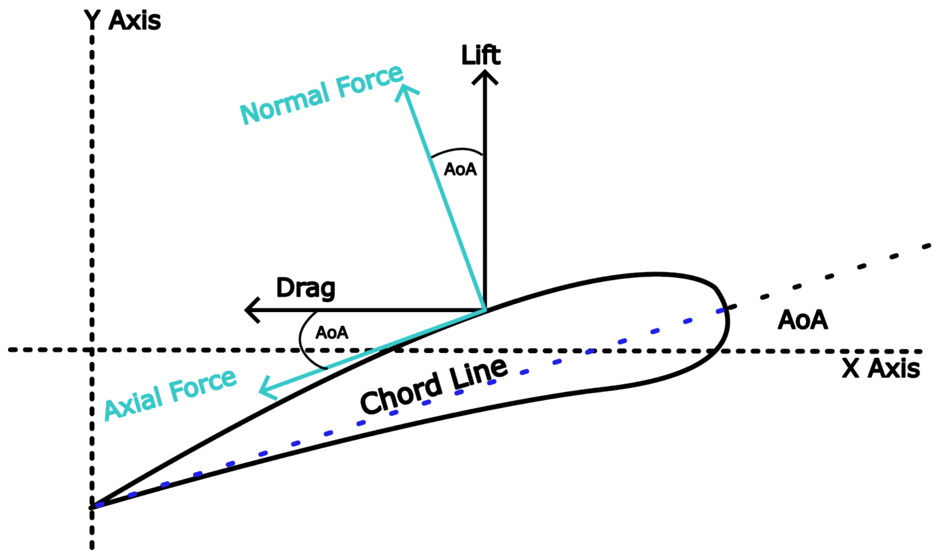

Fig. 3 Lift and drag forces for an airfoil

Additionally, lift and drag are vectors, with components from normal (perpendicular) and axial (along the chord line) forces on the airfoil, due to the non-zero angle of attack. The vector relationship for lift and drag forces is provided in Figure 3. The ratio of the calculated lift-to-drag forces (L/D) can then be determined using equations 1 & 2.

$$L = Ncos(\alpha) - Asin(\alpha) \tag{1}$$

$$D = Nsin(\alpha) + Acos(\alpha) \tag{2}$$

Equations 1 and 2 can also be understood in terms of pressure fields, as airfoils are governed by pressure distributions. Lift occurs when the pressure above the airfoil is lower than the pressure below it, resulting in a net upward force. Similarly, drag is the result of pressure acting against the airfoil's leading edge, opposing horizontal movement. This is explained using an energy balance through Bernoulli's Equation for incompressible flow (see equation 3).

$$p_1 + (\rho_1 v_1^2)/2 = p_2 + (\rho_2 v_2^2)/2 \tag{3}$$

The symbols in equation 3 represent pressure (p), fluid density (ρ), and fluid velocity (v), with subscripts indicating two sides of a system. The law of conservation of energy, as indicated by the equal signs, must hold for both the top and bottom of the airfoil. The equation states that a faster-moving fluid on one side of the airfoil corresponds to a lower pressure, maintaining a constant term; similarly, a slower-moving fluid requires higher pressure to remain constant. These differences in pressure and velocity result in lift and drag.

In aerodynamics, lift, drag, and pressure are typically expressed in terms of non-dimensionalized coefficients. This practice improves understanding of fluid behavior around various objects when the correct non-dimensional values are applied. A key non-dimensional coefficient is the coefficient of pressure (Cp). According to Bernoulli's Equation, dynamic pressure is given by $\rho v^2/2$, representing the pressure from moving air. The free stream pressure is the bulk pressure of the fluid, often one atmosphere, while static pressure refers to the pressure of stationary air close to the surface [11]. A negative Cp indicates a region with less local pressure than the bulk fluid pressure, typically above the airfoil; conversely, a positive Cp indicates higher pressure, typically below the airfoil [12]. Cp is plotted against the non-dimensional chord length to estimate airfoil performance. The definition of Cp is provided below in equation 4.

$$Cp = \frac{p - p_\infty}{\frac{1}{2}\rho v^2} \tag{4}$$

The coefficient of lift (Cl) and drag (Cd) are integral for studying airfoil efficiency. The definitions for Cl and Cd are provided in equations 5 and 6, where A_W is the wetted area.

$$Cl = \frac{L}{\frac{1}{2}\rho v^2 A_W} \tag{5}$$

$$Cd = \frac{D}{\frac{1}{2}\rho v^2 A_W} \tag{6}$$

A drag polar graph, plotting Cl against Cd, can show the maximum slope from the origin to determine the L/D ratio. This graph often includes data from various conditions governed by Reynolds Number (Re). Thus, it can illustrate how the airfoil's performance changes with different parameters. Understanding Re is indispensable for analyzing airfoil behavior.

$$Re = \frac{\rho v L}{\mu} \tag{7}$$

Re is generally defined in equation 7 with a characteristic length (L), fluid velocity(v), and fluid density(ρ), divided by the fluid's dynamic viscosity (μ). This calculation results in a non-dimensional number that governs flow behavior. At low Re values (less than $5 * 10^5$ for external flow), the fluid exhibits predictable laminar flow. However, at Re values above $5 * 10^5$, the flow becomes unpredictable, leading to turbulent flow. Both laminar and turbulent flows are necessary for proper airfoil performance.

Proper contextualization of fluid behavior requires introducing the Mach number, which is another non-dimensional value defined as a ratio of the object's speed over the speed of sound. The speed of sound is defined as $a = \sqrt{\gamma RT}$ in which a is the speed of sound, gamma is the ratio of specific heats, R is the gas constant, and T is the absolute temperature. Calculating the local Mach number near the airfoil is essential to understanding the flow. The two main flows governed by the Mach number are incompressible and compressible flow. Incompressible flow occurs when the density of the fluid is constant because the fluid does not produce significant pressure gradients (i.e., slope). Recall that the ideal gas law states that $p = \rho RT$ where p is pressure and rho is density. Therefore, pressure gradients and density are constant for incompressible flow. Compressible flow is subject to significant pressure gradients that cause the density to vary. This variation in pressure can lead to the presence of shock waves which occur when the object moves faster than the speed of sound or when the Mach value is one. The presence of shock waves is accompanied by abrupt changes in pressure and density [13]. Studying the above concepts is done through the use of computational models on an airfoil; one method used is the finite volume method (FVM).

C. Computational Modeling of 3D Meshes

Jameson and Caughey describe the FVM through the use of primary and secondary cells [14]. These "cells" are finite volume cubes that form part of the computational domain and are constrained to warp around the surface of interest (i.e., an airfoil). By having the cells conform to the shape of the surface, the computer is then instructed to determine the flux through the secondary cells. The secondary cells lie within the primary cell (that is on the surface) but the purpose of the secondary cells is to calculate the flux, such as with a fluid moving around the surface [14]. We can see an example of this in Figure 4.

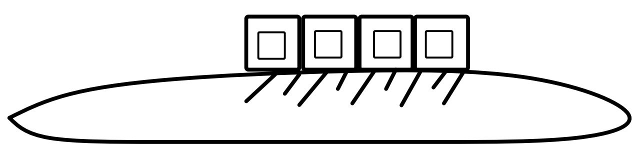

Fig. 4 Primary and secondary cells around an airfoil

The basic premise described above is the Staggered Box Scheme which fills the computational space with these basic units to understand the change in flux around the surface. It must be noted that there is a difference between the basic units in the computational space and the physical space. Those cubes that are in the physical space need to warp to some degree to properly create a mesh around the structure. This warping is mathematically related to the computational space through transformation formulas that relate the mesh points and their movement (shown in Equation 8).

$$x = 8\sum_{i=1}^{8} x_i(\frac{1}{4} + X_i X)(\frac{1}{4} + Y_i Y)(\frac{1}{4} + Z_i Z) \tag{8}$$

Equation 8 assumes the mapping is trilinear meaning that X, Y, and Z are within negative one-half to positive one-half such that the vertices denoted by the subscript i are at plus or minus one-half [14]. Following this structure preserves continuity at the boundary between each basic unit [14]. In turn, this allows for the correct calculation of flux and other transport phenomena.

III. Approaches and Objectives

The first objective of the study is to increase the L/D ratio of the ERJ-145's wings to promote fuel efficiency. The second objective is to provide general insights into the aerodynamics of the jury, strut, and wing, specifically concerning the coefficient of pressures, L/D ratio, and 3D flow visualization. The third objective is to present useful non-dimensional variables that facilitate the parametric study of TBWs. The goals above can be achieved by focusing on the pressure coefficient.

The study of airfoils primarily focuses on the coefficient of pressure, a standard metric for assessing airfoil performance. This information is crucial for designing TBWs, especially beyond Ma 0.3 where compressibility effects become significant. Additionally, the coefficient of pressure is used to derive other parameters: lift, drag, and pitching moment coefficients [12]. Focusing on the coefficient of pressure provides valuable insights into non-uniform pressure distributions on the airfoil which can guide future design decisions. Additional insights can be derived through the study of the boundary layer of the airfoil.

In considering the boundary layer, it's important to examine how flow separates from the airfoil. Kapania et al noted that Mach numbers greater than 0.85 result in flow separation, limiting the study's scope [3]. Therefore, this study focuses on a range of Mach numbers similar to Kapania et al's, from 0.2 to 0.8. Flow separation is identified using the coefficient of pressure versus non-dimensional chord length to observe abrupt changes in pressure gradients, indicative of shock waves [12].

Finally, it's important to note that this study focuses solely on the lifting surfaces of the TBWs as opposed to a simulation of the entire airplane. The lift surfaces include the wings, truss, and jury struts.

IV. Methods

The wing's architecture is constructed using `OpenVSP`, an open-source parametric aircraft modeling tool. OpenVSP allows users to replicate key aircraft geometry: wingspan, chord length, aspect ratio, and more. In this study, OpenVSP is used to create a modified Embraer ERJ-145 wing using the NACA 4412 airfoil. One advantage of using OpenVSP is the ability to incorporate different types of airfoils (e.g., NACA 4412 or 2412) and create CFD meshes. The creation of CFD meshes is essential to running simulations on the airfoil through solvers like SolidWorks Flow Simulation (SFS).

A. SolidWorks Flow Simulation

SFS is a computational fluid mechanics solver that utilizes a Cartesian mesh as described by Jameson and Caughey [14]. SFS achieves an understanding of the system by having three main categories of basic volume elements: solid cubes, fluid cubes, and partial cubes (i.e., those at the boundary of the surface) [15]. Mesh generation is done through the Delaunay triangulation method. This method allows for a mesh to be created without small angles and small triangles [16]. Having too many small triangles in the mesh can produce an over-refinement of the geometry resulting in poor convergence.

The primary advantage of using Cartesian-based mesh generation is that the model information is used in generating the mesh allowing for increased computational speed [15]. Additionally, the implementation of the mass, momentum, and energy conservation laws allows SFS to deal with both incompressible and compressible flows. Furthermore, the SFS package implements key assumptions of the Prandtl Boundary Layer Theory. Potential flow is assumed to exist far from the surface, while viscous effects are considered only in the region close to the surface [17]. The Prandtl Boundary Layer Theory is incorporated into the SFS assuming a thin boundary layer when there are not enough mesh cells to accurately solve the Navier-Stokes equation. However, when there is an excess of mesh cells the boundary layer has a "thick" assumption allowing for accurate computation [15].

The utility of implementing SFS is the user-friendly GUI interface coupled with the robust capabilities to run parametric studies, optimization studies, and define custom parameters like the local skin friction coefficient. The workflow for running the different simulations is shown in Figure 5.

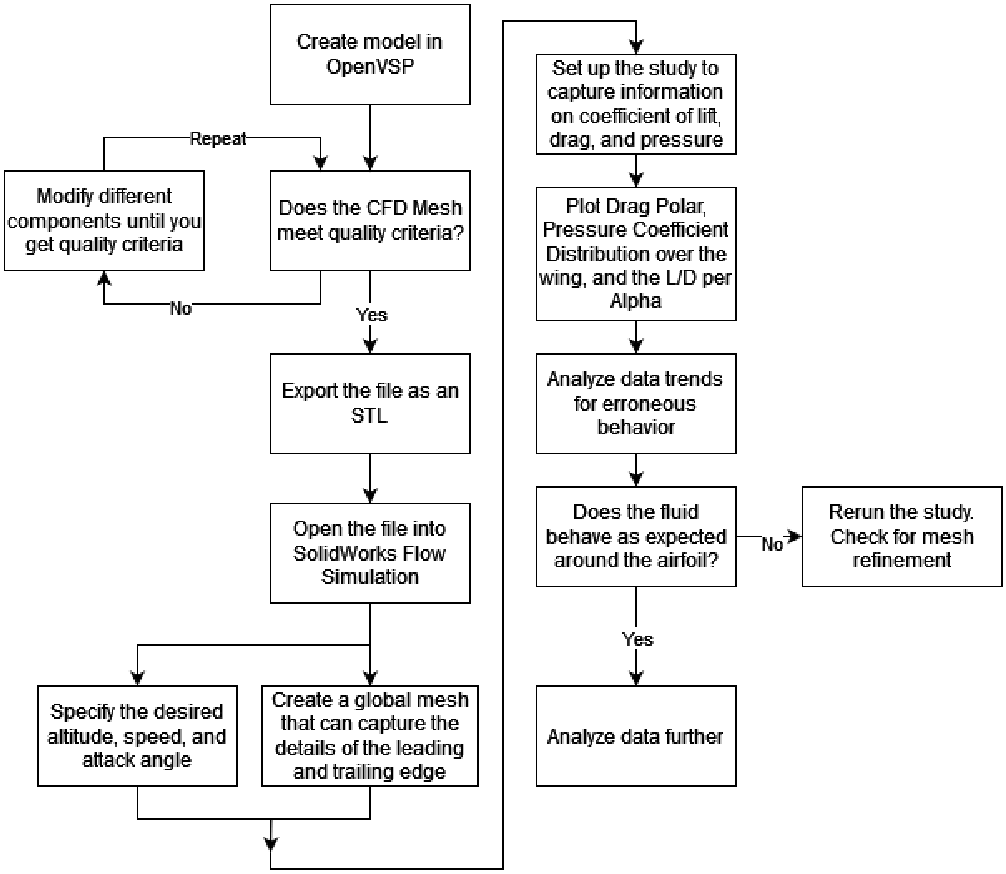

Fig. 5 Framework for studying TBWs

Using the framework shown in Figure 5, a preliminary study is conducted to understand the impact of mesh size on the accuracy of the results. For this effort, a setup similar to that outlined in Heffley's work using the NACA 4412 airfoil is employed (See Figure 7). After completing the simulation using the specified settings, the results were compared with Heffley's wind tunnel data [18].

B. Design of the Datum Wing & Truss Braced Wing

The creation of the datum wing is based on the specifications listed by Frawley which includes the wing's span, area, and aspect ratio [19]. There is no mention of the used airfoil or sweep angle; the NACA 4412 airfoil is chosen due to its widespread use in research and the availability of public data for validation purposes. Additionally, the sweep angle is set to thirty-five degrees, based on a common research model from NASA that is representative of a commercial aircraft [20]. The finalized values are seen in Table 1.

Span [m]	20.04
Sweep [Deg.]	35
Aspect Ratio	7.887
Wing Area [m^2]	51.2
Airfoil	NACA 4412

Table 1 Datum wing design parameters

C. Non-Dimensionalization Approach to TBW

A non-dimensional approach is used to study the flow around the TBW to provide general insights. Additionally, this approach reduces the number of simulations needed to develop a comprehensive understanding of the system. The non-dimensionalization process involves metrics utilized by Bhatia et al [21]. The key metrics include wing sweep angle, truss sweep angle, wing span, wing aspect ratio, truss aspect ratio, and truss span location. These metrics are chosen for their ability to provide a robust understanding of how both the truss and wing contribute to lift and drag and how pressure is distributed. A diagram illustrating the spatial relationships is shown in Figure 6.

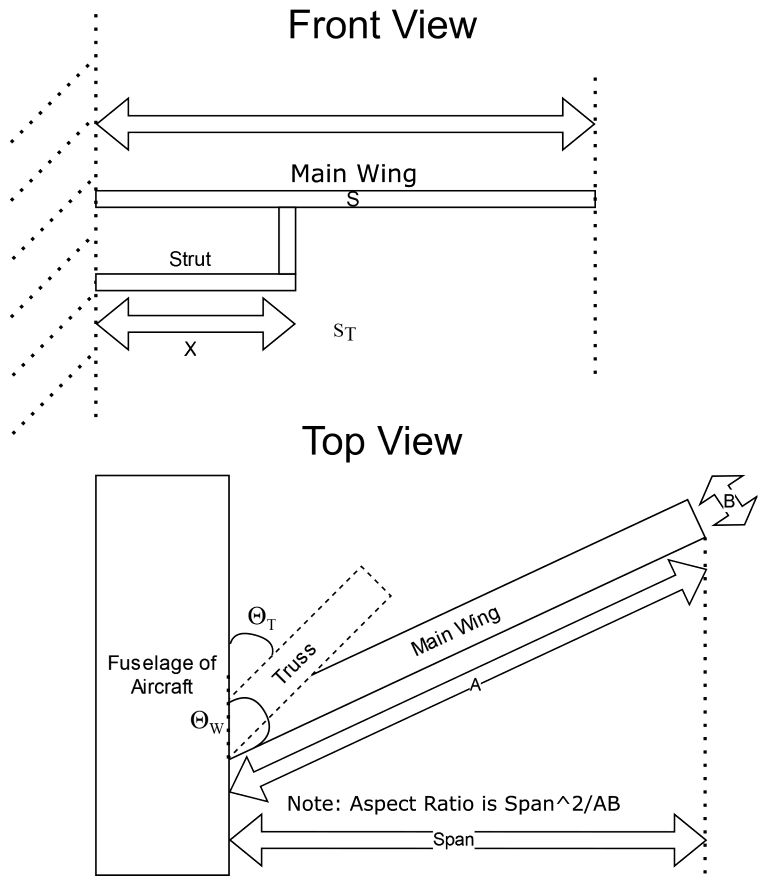

Fig. 6 Spatial relationships used to study TBWs

The selection of these metrics also facilitates comparisons with existing literature. For instance, the ratio of the sweep angle between the wing and truss could be compared with the results of Seber et al [6]. Table 2 summarizes the variables explored and provides clarification on the definitions for the variables in conjunction with Figure 6.

	Variable	Nomenclature	Units	Equations
1	Location in X/Span -Truss	S_T	N/A	X/S
2	Aspect Ratio -Wing	AR_W	N/A	$Span^2/(A*B)$
3	Aspect Ratio - Truss	AR_T	N/A	$Span^2/(A*B)$
4	Sweep Angle - Wing	θ_W	Degrees	N.A.
5	Sweep Angle - Truss	θ_W	Degrees	N.A.

Table 2 Non-dimensional parameters used to study TBWs

V. Results

A. SolidWorks Validation using Wind Tunnel Data

To validate the use of SFS, conditions are set up to mimic Heffley's study on the NACA 4412 airfoil [18]. By replicating the experimental conditions, the simulated data can be compared to the experimental wind tunnel data shown in Figure 7.

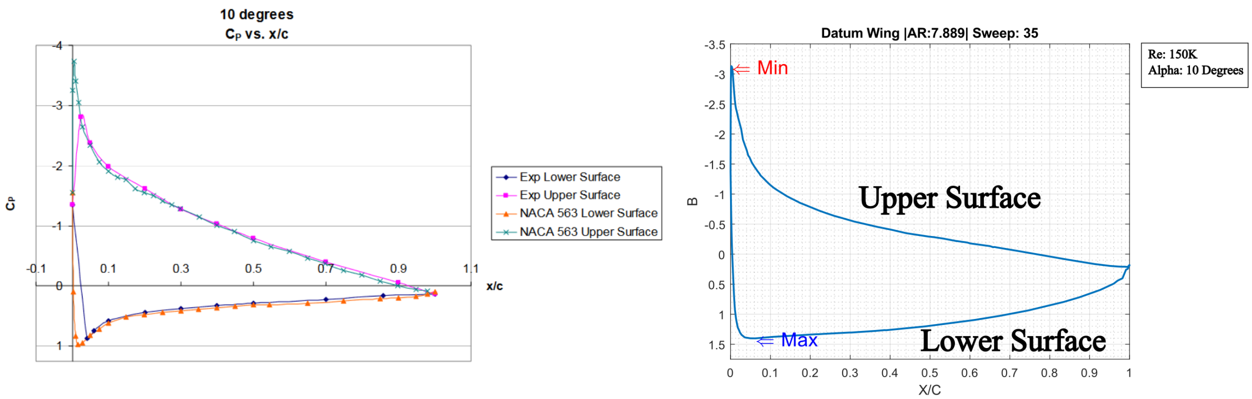

Fig. 7 Comparison with Heffley's wind tunnel data for NACA 4412 [18]

Figure 7 displays the non-dimensional length along the x-axis versus the pressure coefficient. The graph on the right shows results obtained through SFS using a 2D computational domain, while the graph on the left presents experimental wind tunnel data from Heffley [18]. In the experiment, a NACA 4412 wing is tested at an angle of attack of ten degrees with a Re of 150,000. Key observations include the lower coefficient of pressure (Cp) values, reaching approximately 1, with the right side slightly higher near 1.5. The overall shape of the curves aligns well, and the maximum values are approximately 3 for both. This indicates that the solver provides data that closely matches the experimental results. This agreement gives confidence in using the solver for the rest of the analysis.

B. Non-TBW Wing

With the SFS package being validated, analysis begins on the datum wing. This initial study on the datum wing provides the reference data used to compare against the TBW condition.

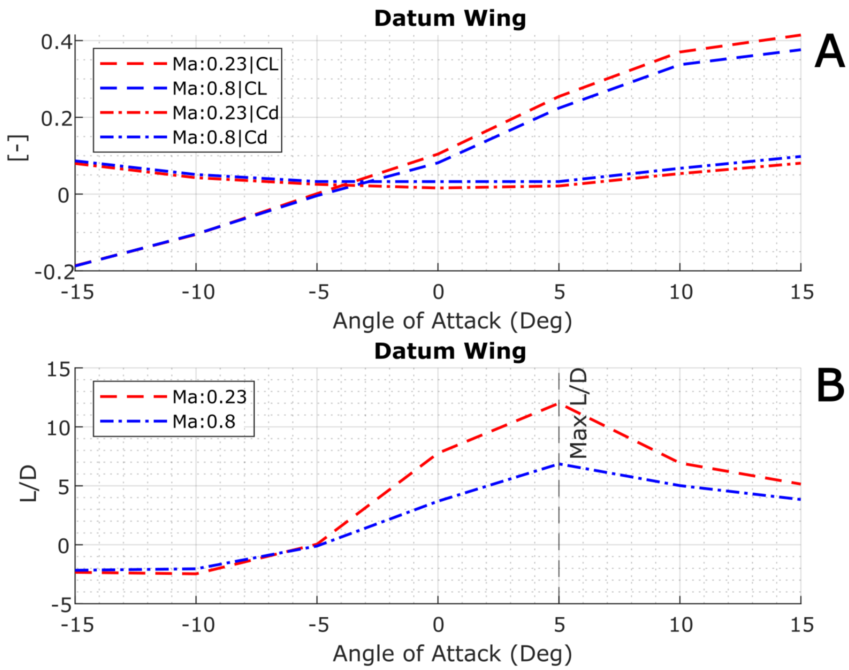

Fig. 8 Datum wing with $\mathbf{AR_W}$: 7.889 and θ_W: 35°

Figure 8A illustrates that the angle of attack is linearly proportional to the lift coefficient under both Mach number conditions. The plot indicates a reduction in rate beyond ten degrees, consistent with aerodynamic theory, which predicts a stall angle at greater angles of attack [12]. The trend in drag is shown to be parabolic, aligning with Heffley's results [18]. Higher drag coefficient values suggest that drag increases with fluid speed due to higher skin friction [22]. Leishman notes that at low angles of attack, changes in the boundary layer are minimal, and viscosity effects are negligible [12]. Consequently, parasitic drag is primarily composed of skin friction. Additionally, higher Mach numbers result in faster fluid movement over the airfoil, significantly increasing shear stress (i.e., skin friction). Thus, parasitic drag is mainly attributed to shear.

Figure 8B shows that the lift-to-drag ratio (L/D) reaches a maximum at five degrees for both Mach conditions. Furthermore, there is a non-linear relationship between the attack angle and L/D. The curve levels off beyond ten degrees due to the approach of the stall angle where flow separation increases. This increased flow separation creates reverse flow conditions that affect the pressure distribution around the airfoil [12]. Additionally, regions of negative lift occur when the angles of attack decrease beyond negative five degrees. This happens because the pressure distribution is inverted; the top of the airfoil experiences higher pressure, while the bottom experiences lower pressure. Therefore, intuitively, this means the aircraft is pushed downwards, which is necessary for landing. Lastly, drag is not dependent on the angle of attack as the flow is always directed at the leading edge.

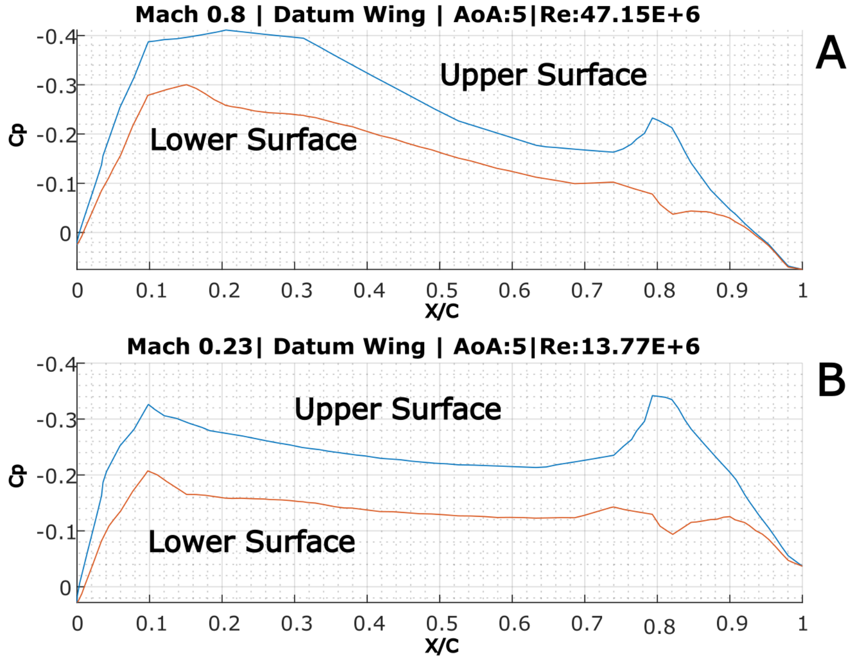

Fig. 9 Pressure distribution of NACA 4412 datum wing at half span

Figure 9 illustrates the coefficient of pressure plotted against the non-dimensionalized chord. The graph demonstrates the reduced pressure region on the top of the airfoil for both the incompressible (Ma: 0.23) and compressible regimes (Ma: 0.8). The leading edge (the values closest to zero) shows that the Cp values are greater than zero in either the Mach 0.23 or 0.8 condition. Therefore, this frontal region is where the fluid is the slowest. As the fluid flows around the airfoil surface the velocities of the fluid change. The top of the airfoil experiences faster air resulting in lower Cp values in comparison to the bottom of the airfoil. The Ma 0.8 condition results in a lower value of Cp compared to the Ma 0.23 condition over the X/C range of 0.3 to 0.8. This observation is explained by the fact that the NACA 4412 is not optimized to fly at the transonic regime.

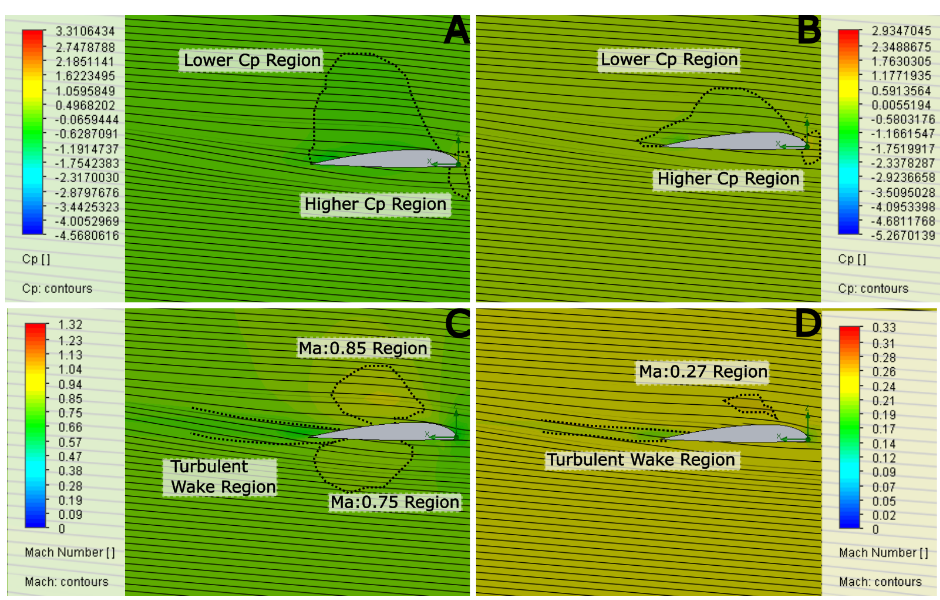

Fig. 10 Aerodynamic visualization of wing with AR_W: 7.889 & θ_W: 35° & AoA: 5°

Figure 10A illustrates a region of lower pressure on the top surface of the airfoil, as expected. Additionally, the higher Cp region on the leading edge reflects the local pressure caused by the fluid pushing against the front of the wing. Similar observations are made in Figure 10B. The streamlines in Figure 10C show the turbulent wake region that forms because the boundary layer separates from the surface of the airfoil. The turbulent wake region is greater in Figure 10C than in Figure 10D. This is expected as a faster flow can cause increased boundary layer separation due to increased adverse pressure gradients in the trailing edge [23]. Conversely, the airfoil in Figure 10D shows a reduced region of turbulent wakes. This is due to the reduced Mach number, which significantly reduces the development of adverse pressure gradients in the trailing edge. The top of the airfoil in Figure 10C & 10D shows the rise in velocity featuring Mach values of 0.85 to 0.94 & 0.24 to 0.27, respectively. The lack of Mach values greater than or equal to one indicates that shock waves are absent in either case.

C. Multi-Variate Analysis

After investigating the aerodynamics of the datum wing, analysis is done on the TBW. The variables of the study are the S_T, aspect ratio, and Mach number. The S_T values of 0.25, 0.5, and 0.75 were chosen to provide general insights into the change in aerodynamics when the truss is closer or farther away from the base of the wing (i.e., close to the fuselage as shown in Figure 6). Similarly, the aspect ratio values are picked to compare the existing value of the ERJ-145 and a higher value. The overview of Mach values of 0.23 & 0.8 corresponds to studying the incompressible and transonic flight regimes.

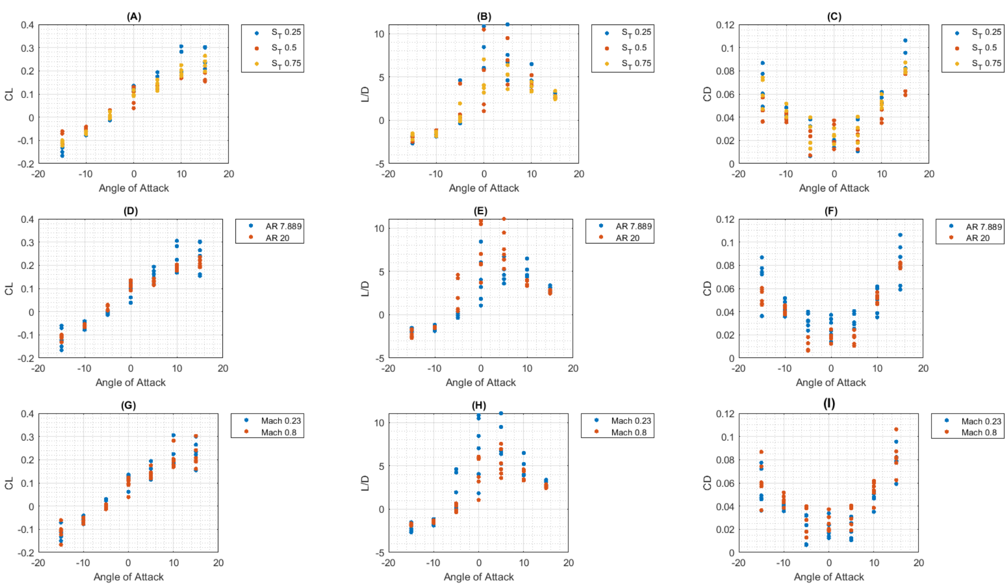

Fig. 11 Group scatter plots by Mach number, aspect ratio, or S_T

1. Coefficient of Lift

In Figures 11A, 11D, and 11G, the linear increase in the lift coefficient with respect to the angle of attack is maintained regardless of the change in S_T, Mach number, or aspect ratio. However, Figure 11A shows that the S_T affects the lift coefficient by reducing its value for the half and three-quarter conditions within the range of five-to-fifteen degrees. Therefore, Figure 11A suggests that the positioning of the strut towards the edge of the wing reduces the coefficient of lift. This is due to the influence of the strut in redirecting flow toward the wing, which can change the pressure distribution (see Figure 13 & 14).

In Figure 11D, the coefficient of lift is lower for the aspect ratio of twenty in the five-to-fifteen-degree range when compared to the 7.889 aspect ratio. However, the higher aspect ratio results in a higher coefficient of lift when the angle of attack is zero. This plot also highlights that the values for the coefficient of lift have a lower range for the higher aspect ratio condition. This observation suggests that higher aspect ratios are desirable regardless of lower values given that a reduced range provides more precision in the design of an aircraft.

In Figure 11G, the coefficient of lift is lower for the Ma 0.8 condition compared to the Ma 0.23 condition within the range of negative-ten-to-ten degrees. This is expected as the NACA 4412 is not designed to operate efficiently in the transonic regime. The NACA 4412 lacks a high radius leading edge coupled with a cambered trailing end [24]. Consequently, this results in increased flow separation that can significantly disrupt the pressure gradient.

2. Lift to Drag

Figure 11B shows that in the negative five-to-ten-degree angle of attack range, the highest L/D values belong to the quarter and half S_T groups. This supports the previous statements that the truss affects the distribution of pressure. As the truss is placed closer to the edge of the wing, there is increased flow redirection to the wing, which affects the coefficient of lift (see Figures 11A & 12). In turn, this impacts the overall L/D. Together with Figures 11A & 12, Figure 11B suggests that there is a benefit to having the truss located between the quarter and half-S_T locations.

Figure 11E shows that the highest values of L/D belong to the higher aspect ratio condition within the range of negative-five-to-five degrees. This is expected as the induced drag is greatly reduced in a higher aspect ratio wing. The reduction in induced drag is caused by the higher aspect ratio wing reducing the intensity of vortices [7]. The reduction in performance in the ten-to-fifteen-degree range is explained by the truss. At the higher angles of attack, there is a redirection of flow to the wings affecting the pressure gradient.

Figure 11H confirms that the NACA 4412 is designed for incompressible conditions as the Ma 0.23 condition has higher values of L/D within the range of negative-five-to-fifteen degrees. It is noted that the range between L/D values decreases at high angles of attack such as ten and fifteen degrees. This observation provides additional support for the truss's effect on changing the flow around the airfoil, which becomes magnified at high angles of attack. Thus, the design of TBWs should consider how the truss can affect flow around the airfoil at various angles of attack to prevent a low stall angle.

3. Coefficient of Drag

Figure 11C demonstrates the parabolic behavior of the drag coefficient with respect to the angle of attack, as shown by Heffley [18]. Additionally, the lowest drag coefficient values are observed in the half S_T condition with the second lowest drag coefficients seen in the quarter S_T condition. This observation supports placing the truss between the quarter and mid-S_T to optimize a reduction of the drag coefficient, resulting in greater values of L/D.

Figure 11F confirms that the overall drag is reduced at higher aspect ratios within the range of negative-five-to-fifteen degrees. Notably, the range for the higher aspect ratio condition is 0.005 and 0.047 for the 7.889 aspect ratio condition at an angle of attack of fifteen degrees. This observation indicates that the range of Cd is reduced across conditions (Mach number & aspect ratio) in higher aspect ratio wings. Therefore, when designing TBW aircraft, it is imperative to use higher aspect ratios, as a lack of drag precision can result in non-uniform lift & drag. This is undesirable as it poses a greater challenge in providing structural support for wings.

Figure 11I provides additional support for the NACA 4412 being unoptimized for transonic flight. The highest values for the drag coefficient are observed in the Ma 0.80 group across all the angles of attack. The increased fluid speed results in increased flow separation, which reduces airfoil performance.

D. Effects of Truss-Flow on Airfoil

After investigating the effects of the design parameters on the lift coefficient, drag coefficient, and L/D, the investigation shifts toward the aerodynamics of the TBWs. Visualizing flow through cut plots enables insight into the flow aerodynamics between the truss and the airfoil. Regions of interest are analyzed to understand why certain parameters have effects on either the lift coefficient, drag coefficient, or L/D.

1. Quarter S_T & Low Aspect Ratio

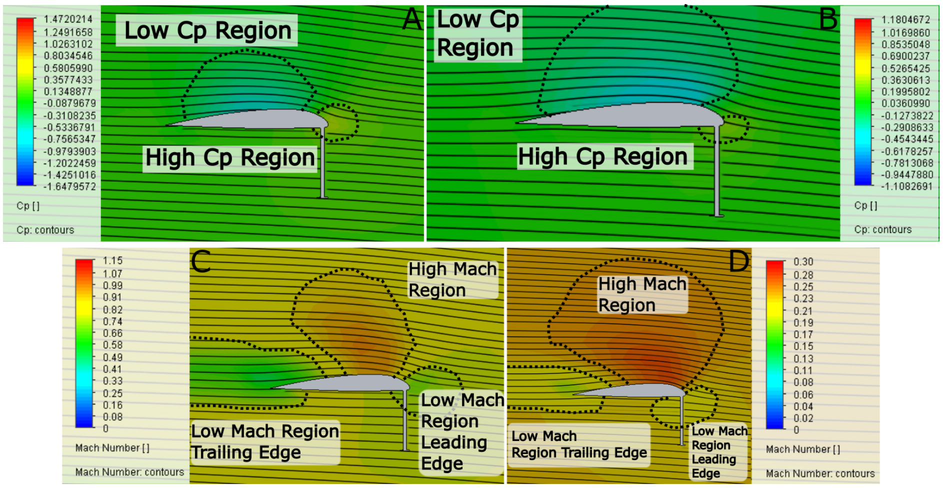

Fig. 12 Aerodynamic visualization of wing with $\mathbf{AR_W}$ & $\mathbf{AR_T}$: 7.889, θ_W & θ_T: 35°, and $\mathbf{S_T}$: 0.25 & AoA: 5°

Figures 12A and 12B both present the characteristic low-pressure region at the top surface of the airfoil. However, the presence of the truss reduces the speed of the air due to the development of the high-pressure region at the leading edge, as shown in Figures 12A and 12B. The presence of the truss also adds additional skin friction, which slows the flow and creates a low Mach region at the leading edge, as shown in Figures 12C and 12D. Therefore, the truss can affect the L/D performance of the airfoil by impacting the fluid behavior at the leading edge. In comparison to the datum wing, the leading edge shown in Figure 12C exhibits approximately a 66% reduction from the 0.75 Mach value of the datum wing. This is important because changes in speed are accompanied by changes in pressure distribution. Consequently, the change in pressure distribution affects the overall behavior of the airfoil.

Furthermore, the trailing edge is affected differently depending on the fluid's speed. In Figure 12C, there is a larger region of lower Mach value fluid compared to Figure 12D. Therefore, at higher Ma values, the truss's effect on reducing the fluid speed becomes more pronounced. The increase in fluid speed in Figure 12C results in increased separation due to an increase in adverse pressure gradients [23]. However, both Figures 12C and 12D show a larger flow separation region compared to the datum wing. This indicates that the truss can affect the aerodynamics of the airfoil by altering the degree of flow separation. This is due to the changing behavior of the fluid at the leading edge, which becomes slower thereby affecting the pressure gradients of the wing.

2. Mid-S_T & Low Aspect Ratio

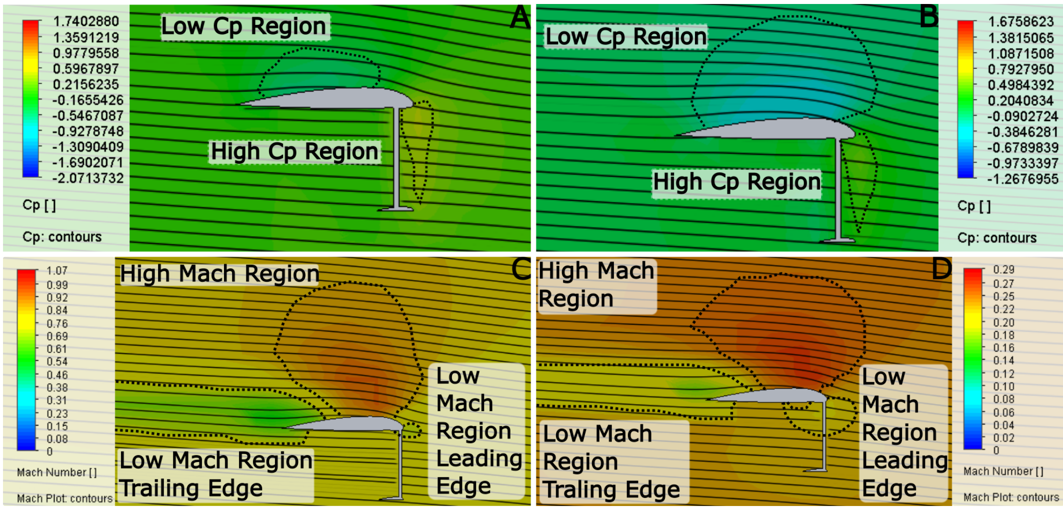

Fig. 13 Aerodynamic visualization of wing with AR_W & AR_T: 7.889, θ_W & θ_T: 35°, and S_T: 0.5 & AoA: 5°

Figures 13A and 13B provide additional support for the assertion that the addition of the truss causes the leading edge to experience higher Cp values. In the datum wing, the Cp value at the leading edge is approximately 0.497, whereas in Figure 13A it is approximately 0.596, an increase of 19.9%. This increase in leading edge pressure is undesirable as it affects the lower Cp region. Moreover, the addition of the truss greatly changes the turbulent wake region; the datum wing in Figure 10C had Mach values of 0.66 to 0.75, whereas in Figure 13C the Mach values range from 0.46 to 0.54, an average decrease of 29.15%. This reduction in speed at the trailing edge can have undesired consequences, such as increased strength of wake vortices [25]. The generation of strong wake vortices is hazardous as it can cause reduced control of the aircraft. Therefore, improvements for future designs of TBWs should focus on reducing the region of slow air near the leading edge to allow the trailing edge region air to speed up, thereby reducing wake vortex strength.

3. Three-Quarter-S_T & Low Aspect Ratio

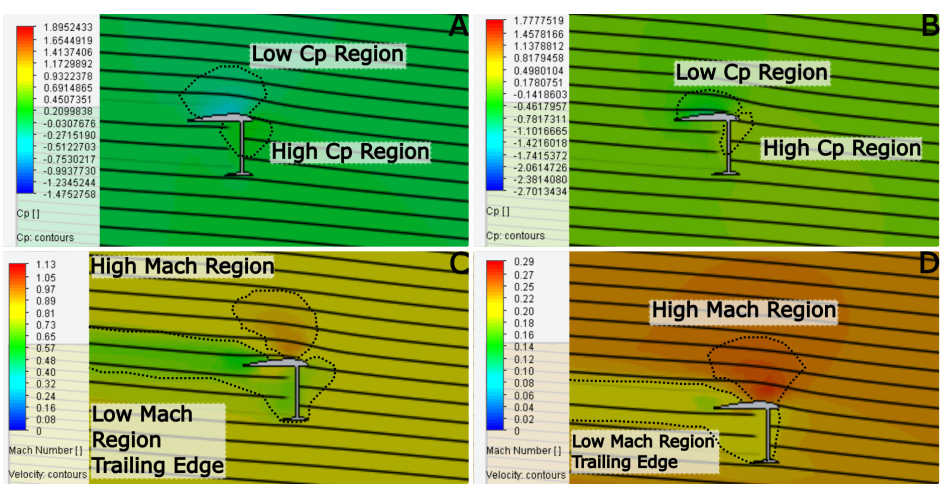

Fig. 14 Aerodynamic visualization of wing with AR_W & AR_T: 7.889, θ_W & θ_T: 35°, and S_T: 0.75 & AoA: 5°

A key takeaway from Figures 14C and 14D is the growth of the low Mach region at the trailing edge. As covered previously, this is undesirable due to an increase in the strength of wake vortices. Compared to the quarter and half S_T, the three-quarters condition is least desirable as it greatly reduces the airspeed. Moreover, compared to the datum wing in Figure 10C, the low Mach region values in Figure 14C are on average decreased by 13.47%. However, although this reduction is numerically less than when compared to Figures 13C and 12C, the low Mach region in Figure 14C is greater in both cases. Therefore, placing the truss towards the edge of the wing is undesirable as it promotes the growth of the region of slow-moving air. Compared to the datum wing, the low Mach region is contained near the trailing edge of the airfoil, which limits the potential for wake vortices to occur along the wing.

Another major observation is the reduction of the pressure gradient as shown in Figures 14A and 14B. This is reflected in the multivariate analysis, which shows that the three-quarters condition had the worst L/D at an angle of attack ranging from negative-five-to-fifteen degrees. Therefore, the position of the strut towards the edge of the wing is undesirable as it diminishes the performance of the airfoil. This is partly due to the increase in local pressure near the leading edge, as Figure 14A has approximately 14% higher Cp values compared to Figure 10A. Therefore, future design should mitigate the increase in local pressure near the leading edge to reduce the low-pressure region Cp values allowing for increased pressure gradients.

4. Quarter-S_T and High Aspect Ratio

Based on the previous analysis that indicated that the three-quarter S_T is less desirable than the quarter and half S_T conditions, further analysis of higher aspect ratios focuses solely on the quarter and half S_T conditions.

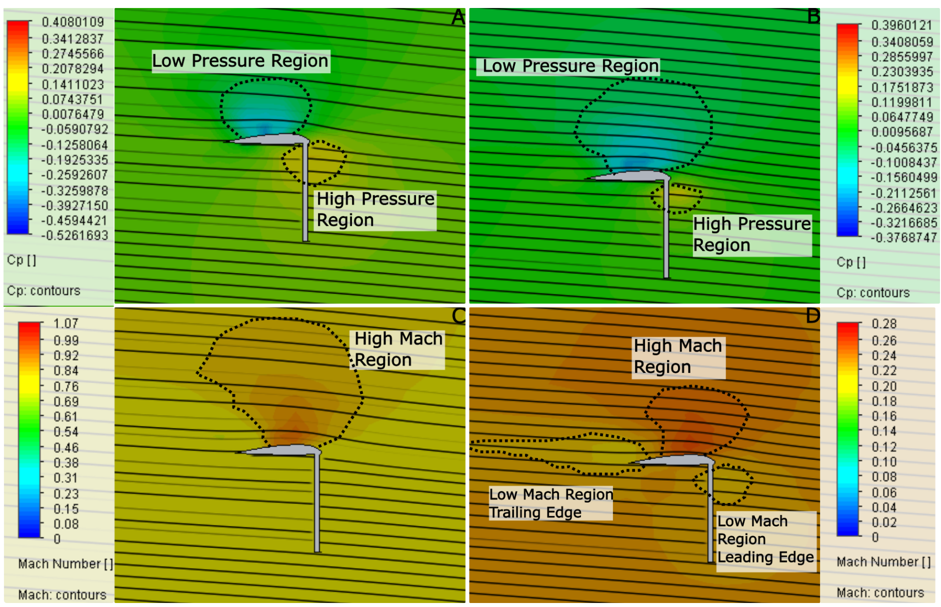

Fig. 15 Aerodynamic visualization of wing with $\mathbf{AR_W}$ & $\mathbf{AR_T}$: 20, θ_W & θ_T: 35°, and $\mathbf{S_T}$: 0.25

Figure 15 features an aspect ratio of twenty. The effect of changing the aspect ratio is the reduction in the magnitude of the Cp values when compared to the datum wing. On average, Figure 15A has an average value of -0.392 Cp for the upper surface, while Figure 10A has an average of -0.628 Cp for the upper surface, indicating a reduction of 37.5%. These results agree with the findings of Shademan and Naghib-Lahouti, who note that in flat plates, a reduction in aspect ratio leads to reduced Cp values [26]. Additionally, the increase in aspect ratio does not affect the growth or shrinkage of the high-pressure region seen in Figures 15A and 15B. Therefore, the graphs support that the truss primarily affects the local pressure increase at the leading edge.

In Figure 15C, the change in the higher aspect ratio allowed the trailing edge region to expand such that it joins up to the leading edge. This effect is also somewhat seen in Figure 15D. However, the lower Mach number allows the two large regions of air to remain separate, preserving the turbulent wake region and leading edge region. Compared to the low aspect ratio and quarter S_T TBW, Figure 15A shows an average Cp of 0.141, while Figure 12A has an average Cp of 0.357, indicating a reduction of 60.5%. Thus, one design solution to improving TBWs without changing the design of the strut is to increase the aspect ratio, as this allows for a reduction in local pressure. In turn, this reduction in local pressure reduces the overall drag of the wing.

5. Mid-S_T and High Aspect Ratio

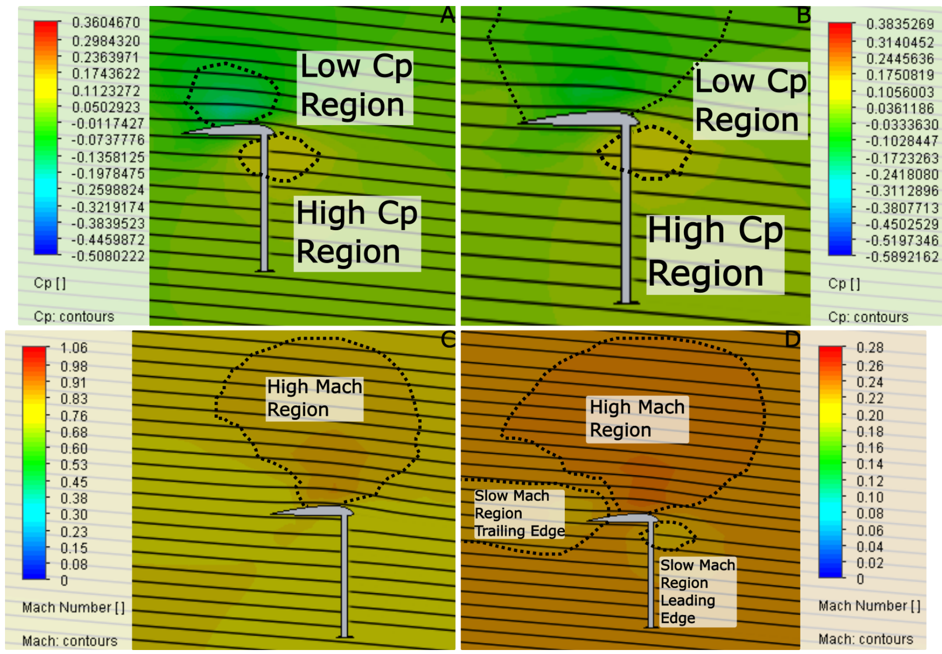

Fig. 16 Aerodynamic visualization of wing with AR_W & AR_T: 20, θ_W & θ_T: 35°, and S_T: 0.5 & AoA: 5°

Figure 16A shows the high Cp region with an average value of 0.143, which is a 71.1% reduction from the average value of 0.496 for the datum wing (see Fig. 10A). Therefore, the increase in aspect ratio reduces the Cp values at the leading edge. This reduction in local pressure is useful for reducing overall drag. Additionally, Figure 16B has an average high region Cp value of 0.14, which is 2.1% less than the high region average Cp value of Figure 16A. This small difference shows that a higher aspect ratio allows for similar Cp values between the incompressible and transonic regimes. Moreover, the Cp values in the low Cp region for Figure 16A average -0.166, whereas for Figure 16B, the values average -0.065. Therefore, the current combination of the truss location and aspect ratio change favors performance at higher Mach values. This insight is used to accommodate different aircraft needs, such as those of an ERJ-145 (compressible regime) or a Cessna 172 Skyhawk (incompressible regime).

Figure 16C shows a lack of a conventional slow Mach region at the trailing edge when compared to the datum wing (see Figure 10C). This behavior requires that the truss be slightly modified to allow better flow through the truss to maintain the three flow regions as seen in the datum wing (see Figure 10 C & D). The change in aspect ratio did not result in Mach values greater than one, which indicates a lack of shock waves. Figure 16D shows the conventional trailing edge, leading edge, and top surface regions. This contrasts with Figure 16C and suggests that higher Mach numbers allow for more homogeneous Mach value regions. Additionally, Figure 10C shows the conventional regions at the trailing edge, leading edge, and top surface. Thus, the addition of the truss and change in aspect ratio alter the behavior of the fluid to combine regions. The danger in allowing this merger of slow air regions is the potential to increase the strength of trailing wakes. Therefore, the aspect ratio and truss position need to be optimized to maintain the classic three regions.

VI. Conclusion

Key Takeaways

- The addition of a truss creates an increase in local pressure near the leading edge. Reduction of this local pressure is done by increasing the aspect ratio.
- The location of the truss is favored towards the quarter and mid-S_T region to optimize performance and increase the precision in Cl and Cd values.
- Combinations of truss location and aspect ratio optimize the performance in either the incompressible or transonic regime.

Improving the sustainability of aircraft is important to reduce carbon emissions. A strategy for improving the sustainability of aircraft is to increase their L/D to reduce fuel consumption. Improving the performance of the wings of an ERJ-145 aircraft is achieved, as the quarter S_T, high aspect ratio condition resulted in an L/D of 7.54 at an AoA of five degrees and Ma of 0.8. In comparison, the datum wing at the same AoA and Ma number has an L/D of 6.85, resulting in an improvement of 10%. Although this percentage seems marginal, it must be noted that it is achieved using the original span of the ERJ-145. Therefore, potential future iterations could look into extending the span, as this improves the L/D value. However, careful consideration must be taken, as increasing the span creates problems with interacting with airport infrastructure.

Moreover, it is determined that the location of the S_T plays a role in affecting the local pressure near the leading edge. It is noted that the reduction in fluid velocity reduced the low-pressure region near the top of the airfoil. However, this effect is reduced when the aspect ratio is increased. Therefore, careful consideration must be taken to balance the aspect ratio and truss location to reach the desired Cp values.

Overall, these findings have implications for guiding the designs of aircraft in incompressible and transonic regimes. In particular, this has applications in increasing the efficiency of electric aircraft, as higher-performing wings can potentially reduce the need for heavy, powerful motors. Additionally, the improvement of transonic aircraft can take two main forms: improvement of existing aircraft or design of new aircraft. The former can prove expensive, as new aircraft licenses must be approved by the Federal Aviation Administration. The latter can potentially result in reduced costs, as the only aspect of validation needed is the addition of the TBWs. In turn, this can accelerate efforts to create more fuel-efficient aircraft, promoting fuel consumption reductions.

Future work will focus on exploring other variables, such as the sweep angle, incorporation of transonic airfoils, and validating the TBW simulated data with experimental data of a 3D-printed model. In particular, the sweep angle being unoptimized for transonic flight reduces the overall performance of the TBW system. Future investigations should look into whether θ_W and θ_T should be equal, as is done in this study. Additionally, validation of these simulated results needs experimental wind tunnel data to ensure model accuracy. Although validation is done on SFS as a CFD solver, more work should focus on SFS validity for complex 3D wing geometry. Lastly, the exploration into using transonic airfoils is imperative to see if the trends observed in this study hold for wings that are more representative of a regional transonic jet.

Acknowledgments

I would like to thank my mentor, Alexander Reaves, for continuously providing insight and mentorship throughout the research process. I would also like to express my heartfelt gratitude to my family and friends, who have provided unwavering support throughout this research journey. Your encouragement, patience, and trust have enabled me to pursue my passion with confidence. Finally, I would like to thank Yale University for making this research project possible by funding the Pembroke Cambridge Summer Program.

References

[1] Zhang, J., Roumeliotis, I., and Zolotas, A., "Sustainable Aviation Electrification: A Comprehensive Review of Electric Propulsion System Architectures, Energy Management, and Control," *Sustainability*, Vol. 14, 2022, p. 5880. https://doi.org/10.3390/su14105880.

[2] Harrison, N., Hoffman, K., Lazzara, D., Reichenbach, E., Sclafani, A., and Droney, C., "Subsonic Ultra Green Aircraft Research: Phase IV Final Report -Volume I Mach 0.80 Transonic Truss-Braced Wing High- Speed Design Report," , 10 2023. URL https://ntrs.nasa.gov/api/citations/20220016017/downloads/NASA-CR-20220016017%20Volume%201.pdf.

[3] Kapania, R. K., Schetz, J. A., Mallik, W., Segee, M. C., and Gupta, R., "Multidisciplinary Design Optimization and Cruise Mach Number Study of Truss-Braced Wing Aircraft," , 06 2018. URL https://ntrs.nasa.gov/citations/20180008436.

[4] Beaven, K. A., "America's Regional Airports Are Disappearing. Who's to Blame?" , 12 2022. URL https://www.tripsavvy.com/the-decline-of-america-s-regional-airports-6890542.

[5] Pfeminger, W., "Laminar flow control laminarization," 1977. URL https://www.semanticscholar.org/paper/Laminar-flow-control-laminarization-Pfeminger/5700fb2c828fa7ed77a271cac5e9bfb940e890f3#citing-papers.

[6] Seber, G., Ran, H., Schetz, J. A., and Mavris, D. N., "Multidisciplinary Design Optimization of a Truss Braced Wing Aircraft with Upgraded Aerodynamic Analyses," *29th AIAA Applied Aerodynamics Conference*, 2011. https://doi.org/10.2514/6.2011-3179.

[7] Benson, T., “Induced Drag Coefficient,” , ???? URL https://www.grc.nasa.gov/www/k-12/VirtualAero/BottleRocket/airplane/induced.html.

[8] Chakraborty, I., Nam, T., Gross, J. R., Mavris, D. N., Schetz, J. A., and Kapania, R. K., “Comparative Assessment of Strut-Braced and Truss-Braced Wing Configurations Using Multidisciplinary Design Optimization,” *Journal of Aircraft*, Vol. 52, 2015, pp. 2009–2020. https://doi.org/10.2514/1.c033120.

[9] Ivaldi, D., Secco, N. R., Chen, S., Hwang, J. T., and Martins, J. R. R. A., “Aerodynamic Shape Optimization of a Truss-Braced-Wing Aircraft,” 2015. https://doi.org/10.2514/6.2015-3436.

[10] Anderson, J., *Fundamentals of aerodynamics.*, 6^{th} ed., Mcgraw-Hill, 2016.

[11] Gracey, W., “Measurement of Aircraft Speed and Altitude,” *ntrs.nasa.gov*, 1980. URL https://ntrs.nasa.gov/citations/19800015804.

[12] Leishman, J. G., “Aerodynamics of Airfoils,” *eaglepubs.erau.edu*, 2022. https://doi.org/10.15394/eaglepub.2022.1066.n23, URL https://eaglepubs.erau.edu/introductiontoaerospaceflightvehicles/chapter/airfoil-characteristics/.

[13] Leishman, J. G., “Mach Number & Reynolds Number,” *eaglepubs.erau.edu*, 2022. https://doi.org/10.15394/eaglepub.2022.1066.n13, URL https://eaglepubs.erau.edu/introductiontoaerospaceflightvehicles/chapter/mach-number-and-reynolds-number/.

[14] JAMESON, A., and CAUGHEY, D., “A finite volume method for transonic potential flow calculations,” *3rd Computational Fluid Dynamics Conference*, 1977. https://doi.org/10.2514/6.1977-635.

[15] Sobachkin, A., and Dumnov, G., “Numerical Basis of CAD-Embedded CFD,” , 2014. URL https://www.solidworks.com/sw/docs/Flow_Basis_of_CAD_Embedded_CFD_Whitepaper.pdf.

[16] Shewchuk, J., “Two-dimensional Delaunay triangulations,” , 2012. URL https://people.eecs.berkeley.edu/~jrs/papers/meshbook/chapter2.pdf.

[17] Subramanian, R., “Elements of Prandtl’s Boundary Layer Theory,” , 2020. URL https://lin-web.clarkson.edu/projects/subramanian/ch490/notes/Prandtl%27s%20Boundary%20Layer%20Theory.pdf.

[18] Heffley, D., “Aerodynamic Characteristics Aerodynamic Characteristics of a NACA 4412 Airfoil of a NACA 4412 Airfoil,” , 2007. URL https://www.baylor.edu/content/services/document.php/41147.pdf.

[19] Frawley, G., *The International Directory of Civil Aircraft 1997/98*, Aerospace Publications Pty Ltd, 1997.

[20] “Model Description | NASA Common Research Model,” , 04 2022. URL https://commonresearchmodel.larc.nasa.gov/home-2/high-speed-crm/experimental-approach/model-description/.

[21] Bhatia, M., Kapania, R. K., and Haftka, R. T., “Structural and Aeroelastic Characteristics of Truss-Braced Wings: A Parametric Study,” *Journal of Aircraft*, Vol. 49, 2012, pp. 302–310. https://doi.org/10.2514/1.c031556.

[22] Leishman, J. G., “Aerodynamics of Finite Wings,” *eaglepubs.erau.edu*, 2023. https://doi.org/10.15394/eaglepub.2022.1066.n24, URL https://eaglepubs.erau.edu/introductiontoaerospaceflightvehicles/chapter/finite-wing-characteristics/.

[23] Leishman, J. G., “Boundary Layers,” *eaglepubs.erau.edu*, 2023. https://doi.org/10.15394/eaglepub.2022.1066.n22, URL https://eaglepubs.erau.edu/introductiontoaerospaceflightvehicles/chapter/introduction-to-boundary-layers/.

[24] Tapee, J., and Zaubi, A., “Transonic Airfoil Testing,” , 2007. URL https://engineering.purdue.edu/~aae520/tapee-zaubi-Transonic-Airfoil.pdf.

[25] FAA, “Aeronautical Information Manual - AIM - Wake Turbulence,” , 03 2024. URL https://www.faa.gov/air_traffic/publications/atpubs/aim_html/chap7_section_4.html.

[26] Shademan, M., and Naghib-Lahouti, A., “Effects of aspect ratio and inclination angle on aerodynamic loads of a flat plate,” *Advances in Aerodynamics*, Vol. 2, 2020. https://doi.org/10.1186/s42774-020-00038-7.